Title
ANGULAR DISTRIBUTIONS FROM MULTIPARTICLE PRODUCTION MODELS

Authors
Lyon, Donald E.
Risk, Clifford
Tow, Don.

Publication Date
1970-07-01

Submitted to Physical Review

UCRL-19884
Preprint

c.2

ANGULAR DISTRIBUTIONS FROM MULTIPARTICLE PRODUCTION MODELS

Donald E. Lyon, Jr., Clifford Risk, and Don Tow

July 1970

AEC Contract No. W-7405-eng-48

DISCLAIMER

ANGULAR DISTRIBUTIONS FROM MULTIPARTICLE PRODUCTION MODELS*

Donald E. Lyon, Jr.

Department of Physics
University of Michigan
Ann Arbor, Michigan 48104

and

Clifford Risk and Don M. Tow

Lawrence Radiation Laboratory
University of California
Berkeley, California 94720

July 9, 1970

ABSTRACT

Using $\exp(-Ap_T^2)(d^3p/E)$ as the momentum distribution of secondaries produced in ultrahigh-energy collisions--a result predicted by the multiperipheral model, by Feynman's parton model, and by Cheng and Wu's consideration of hadrons as extended objects with many internal degrees of freedom--we obtain the characteristic features of the angular distribution. We discuss the dependence on incident energy, mass of secondaries, and the value of A. We find that the c.m. angular distribution in the variable $\eta_{cm} = -\ln \tan(\theta_{cm}/2)$ has a two-bump structure, whereas the lab angular distribution in $\eta = -\ln \tan \theta_\ell$ is flat. This difference leads us to a discussion of the transformation between c.m. and lab angular distributions. We find that the usual relativistic approximation of the exact transformation leads to incorrect results. Finally, we show that these momentum and angular distributions approach limiting distributions.

In the last two years advances have been made in the development of theoretical models of multiparticle production in high-energy collisions. The multiperipheral model (MPM) of ABFST[1] has been revived and studied in the form with elementary pion exchange[2] as well as the form with Reggeized meson exchange.[3] Further developments have been made by Feynman[4] with his parton model, and by Cheng and Wu[5] through the study of Feynman diagrams. At the same time, the Michigan-Wisconsin collaboration[6] has collected ≈800 interactions of cosmic ray hadrons in liquid hydrogen, in the range 100 to 800 GeV. Among other things, they measured the angular distribution of the produced secondaries.[7] These new data have offered the opportunity to test the predictions made by these models regarding angular distributions. In an earlier work[8] this test was performed. In this paper we explore in detail the characteristic features of the angular distribution predicted by these theoretical models.

Rather than be constrained by the specific features of any one model, we discuss the general features common to all three models. They all predict that the momentum distribution of the secondaries is given by[9]

$$d^3N = e^{-Ap_T^2} \frac{d^3p}{E}, \tag{1a}$$

and hence that the double differential momentum distribution is given by

$$\frac{\partial^2 N}{\partial p_L \partial p_T} = \frac{p_T e^{-Ap_T^2}}{\left(p_L^2 + p_T^2 + m^2\right)^{1/2}} . \tag{1b}$$

Here, p_L and p_T are the longitudinal and transverse momentum components of the secondary, m is its mass, and E is its energy. Of course, this distribution does not hold for all secondary momenta up

to the kinematical boundary because of phase space effects. The overall delta function of energy-momentum conservation modifies the distribution near the boundary, and, hence, Eq. (1) holds only for secondaries sufficiently far from it. For example, in the center-of-momentum system (see Fig. 1a) we expect the distribution (1) to hold inside the region 2 - 3, with modifications outside. In the laboratory system (see Fig. 1b) we expect the distribution (1) to hold inside the region 2' - 3', with modifications outside. [We emphasize that (1) holds only for the produced secondaries; the incident particle, which has an elasticity ≈ 0.5, must be handled separately.]

It is not hard to anticipate the general features of the angular distribution predicted by Eq. (1). In the lab system Eq. (1) is valid over some range $0 \ll p_L \ll p^{\ell}_{max} \approx s/2$, where s is the center-of-mass energy squared. Since the transverse momentum distribution is peaked about some small value p_{TO}, and since in the lab $p_L \gg p_{TO}$, the lab angle, θ_ℓ, of emission of secondaries relative to the beam direction will be predominantly small. This leads us to use the variable η :

$$\eta \equiv -\ell n \tan \theta_\ell \qquad (2)$$
$$= \ell n \frac{p_L}{p_T} \approx \ell n \frac{p_L}{p_{TO}} ,$$

which stretches the θ_ℓ axis in the region of interest.[10] Then, noting that in the lab system $p_L \approx E$ for the secondaries in the range of validity of Eq. (1), we obtain

$$\frac{\partial N}{\partial \eta} \approx \frac{\partial N}{\partial [\ell n (p_L/p_{TO})]} = p_L \frac{\partial N}{\partial p_L} \approx \text{constant} .$$

Therefore, the η distribution is flat over the range of η corresponding

to the p_L from region 2' - 3' of Fig. 1b, and drops to zero on either side.

In the center-of-momentum system, Eq. (1) is valid over the symmetric region $|p_L| \ll p^c_{max} \approx s^{1/2}/2$, and the peaking of p_T now leads predominantly to forward-backward emission. Hence we use the variable η_{cm},

$$\eta_{cm} = - \ell n \tan \frac{\theta_{cm}}{2} , \tag{3}$$

where θ_{cm} is the c.m. angle of emission of secondaries relative to the beam. The regions $p_L \approx \pm E$ now give two flat sections in the η_{cm} distribution that are located on either side of $\eta_{cm} = 0$ ($\theta_{cm} = 90$ deg), with some other behavior around $\eta_{cm} = 0$. For η_{cm} near the kinematical boundary, the distribution drops to zero.

These general features can be seen in detail by deriving a closed form for the angular distribution. We begin with the center-of-momentum system, and, as a first approximation, we neglect the phase-space modifications to Eq. (1). Changing variables to $p = (p_L^2 + p_T^2)^{1/2}$ and η_{cm}, we obtain from (1b)

$$\frac{dN}{d\eta_{cm}} = \frac{1}{\cosh^2 \eta_{cm}} \int_0^{p^{cm}_{max}} \frac{p^2}{(p^2 + m^2)^{1/2}} \exp\left(\frac{-Ap^2}{\cosh^2 \eta_{cm}} \right) dp . \tag{4}$$

Integration leads to

$$\frac{dN}{d\eta_{cm}} = \frac{1}{2A} \left\{ x\, e^x \left[K_1(x) - K_0(x) \right] - \exp\left[-2x(p^{cm}_{max}/m)^2 \right] \right\} , \tag{5}$$

where $x = \frac{1}{2}(m^2 A/\cosh^2 \eta_{cm})$ and K_0, K_1 are modified Hankel functions. For large η_{cm} (but small enough so that $e^x \gg \exp[-2x(p^{cm}_{max}/m)^2]$), K_1 dominates Eq. (5) and gives a flat distribution, independent of m. When $\cosh^2 \eta_{cm} \approx A(p^{cm}_{max})^2$ [i.e., when $\eta_{cm} \approx \ell n(A^{1/2}\, p^{cm}_{max})$], the first and third terms cancel and the distribution drops to zero. The width of the distribution is therefore proportional to $\ell n\, p^{cm}_{max}$ or to $\ell n\, s$. Figure 2a shows the η_{cm} distribution for several values of p^{cm}_{max}, with A and m fixed, and Figs. 2b, 2c illustrate the dependence on A and m when p^{cm}_{max} is fixed. We see that the distribution has a two-bump structure, with the dip at $\eta_{cm} = 0$ proportional to A and m. Finally, from Fig. 1a we know that the correct distribution (with phase-space effects included) deviates from Eq. (5) for large $|\eta_{cm}|$ (i.e., for large $|p_L|$); but the deviations occur at the ends of the distribution and do not change the shape of the internal portion (see Fig. 1c).

In the lab system, because Eq. (1) is invariant under a z boost (z is the beam direction), the distribution in the lab variable $\eta_\ell \equiv -\ell n \tan(\theta_\ell/2)$ is again given by Eq. (4):

$$\frac{dN}{d\eta_\ell} = \frac{1}{\cosh^2 \eta_\ell} \int_0^{p^\ell_{max}} \frac{p^2}{(p^2 + m^2)^{1/2}} \exp\left(\frac{-Ap^2}{\cosh^2 \eta_\ell}\right) dp \,. \tag{4'}$$

However, as previously discussed, the energy-momentum conservation δ function now restricts the region of validity of Eq. (1) to some positive range (i.e., $\eta_\ell > 0$) so that the η_ℓ distribution is just the right-hand portion of the η_{cm} distribution, stretched by the larger $p^\ell_{max} \approx s/2$. Here the phase-space effects cause the correct distribution

to deviate from Eq. (4') in the regions of small p_L and very large p_L (i.e., for $\eta_\ell \approx 0$ and large η_ℓ). The η_ℓ distribution is therefore a single-dump distribution (see Fig. 1d). The $\eta \equiv -\ell n \tan \theta_\ell$ distribution, which is related to the η_ℓ distribution by a Jacobian that effectively stretches the η_ℓ axis, is then also a single-bump distribution (see Fig. 3).[11]

The difference between the η_{cm} and η distributions (the two-bump structure of $dN/d\eta_{cm}$ and the single-bump structure of $dN/d\eta$) shows that a relativistic approximation that has often been used to transform angular distributions from lab to c.m. can give misleading results. This transformation states that the $dN/d\eta$ and $dN/d\eta_{cm}$ distributions are related by a simple translation of the η axis by an amount $\ell n\, \gamma$. This comes about in the following way: The angles θ_ℓ and θ_{cm} are related by

$$\tan \theta_\ell = \frac{1}{\gamma_c} \frac{\sin \theta_{cm}}{\cos \theta_{cm} + \beta_c/\beta}, \tag{7}$$

where β is the velocity of the secondary in the c.m. and β_c is the velocity of the c.m. relative to the lab $\left[\gamma_c = (1 - \beta_c^2)^{-1/2}\right]$. For large incident energy $\beta_c \approx 1$; if the secondary is also relativistic, then $\beta \approx 1$ and one obtains

$$\tan \theta_\ell \xrightarrow[\frac{\beta_c}{\beta} \to 1]{} \frac{1}{\gamma_c} \tan \frac{\theta_{cm}}{2} \tag{8a}$$

or

$$\eta = \ell n\, \gamma_c + \eta_{cm}. \tag{8b}$$

However, from our derivations of the correct distributions (Figs. 2a, 3),

we know that this transformation cannot be valid. This can be understood by examining a c.m. Peyrou plot generated from the distribution (1) (see Fig. 4). Note that in this plot many secondaries populate the region near the origin, and hence are nonrelativistic. The relativistic transformation (8) cannot hold for them; they must be transformed by the exact transformation (7).

Cosmic-ray physicists experimentally measure the angular distribution (lacking momentum analysis) of secondaries in the lab; then they often use the transformation (8) to get the "experimental" c.m. angular distribution and compare with various theoretical models. As we have shown, this relativistic transformation is a poor approximation. Therefore, a better approach is to develop theoretical models in the lab and compare directly with the measured lab data. If some theoretical models, such as the two-fireball model,[12] are most naturally formulated in the c.m., then one should transform to the lab without using this relativistic approximation. One method is to specify the c.m. momentum distribution in the model, and transform it exactly into the lab by Eq. (7). For example, in Ref. 8, the c.m. momentum distribution was Monte Carloed, and the individual secondaries generated were transformed into the lab by Eq. (7).

The possibility of a simple transformation between the lab and c.m. is retained by using a variable w, called rapidity, which was recently introduced by Feynman:[4]

$$w = \tanh^{-1}\left(\frac{p_L}{E}\right) = -\ell n\left[\frac{E - p_L}{(p_T^2 + m^2)^{1/2}}\right] . \qquad (9)$$

This variable satisfies

$$w_{cm} = -\ell n \left(\frac{1-\beta}{1+\beta}\right)^{1/2} + w_{lab} . \qquad (12)$$

(In the limit of $p_T^2 \gg m^2$, w reduces to $-\ell n \tan \frac{\theta}{2}$.) Using this variable and the distribution (1), we obtain a flat distribution for dN/dw in both the c.m. and the lab systems that scales with $\ell n\ s$ (see Fig. 5). When experiments are done with storage rings or at the National Accelerator Laboratory, where momentum distributions can be measured, the Feynman rapidity variable should replace the usual $\ell n \tan \theta$ variables.

Finally, since the distribution (1) is derived for large s and is independent of s, it obviously satisfies the hypothesis of limiting fragmentation.[13] This hypothesis states that the momentum distribution of secondaries in any definite region of phase space approaches a limiting distribution as $s \to \infty$. Furthermore, the momentum distribution (1) also leads to a limiting angular distribution; in Fig. 2a we see that the distributions, except for end effects, approach the same value. This approach to a limit at smaller η comes about from the sharp p_T cutoff of Eq. (1).

FOOTNOTES AND REFERENCES

* This work was supported by the U. S. Atomic Energy Commission and the National Science Foundation.

1. L. Bertocchi, S. Fubini, and M. Tonin, Nuovo Cimento 25, 626 (1962); D. Amati, A. Stanghellini, and S. Fubini, Nuovo Cimento 26, 896 (1962).

2. J. S. Ball and G. Marchesini, Phys. Rev. 188, 2508 (1969); D. M. Tow, Some Predictions of the ABFST Multiperipheral Model (Lawrence Radiation Laboratory Report UCRL-19449, 1970), Phys. Rev. (to be published); G. F. Chew, T. W. Rogers, and D. R. Snider, Relation Between the Multi-Regge Model and the ABFST Pion-Exchange Multiperipheral Model (Lawrence Radiation Laboratory Report UCRL-19457, 1970), Phys. Rev. (to be published).

3. G. F. Chew and A. Pignotti, Phys. Rev. 176, 2112 (1968); G. F. Chew, M. L. Goldberger, and F. E.Low, Phys. Rev. Letters 22, 208 (1969); I. G. Halliday, Nuovo Cimento 60A, 177 (1969); I. G. Halliday and L. M. Saunders, Nuovo Cimento 60A, 494 (1969); P. D. Ting, Studies of Multiperipheral Integral Equations, Lawrence Radiation Laboratory Report UCRL-19802, 1970, to be submitted to Phys. Rev.; and many others.

4. R. P. Feynman, The Behavior of Hadron Collisions at Extreme Energies, in High Energy Collisions--Third International Conference (Gordon and Breach, 1969).

5. H. Cheng and T. T. Wu, Phys. Rev. Letters 23, 1311 (1969).

6. L. W. Jones et al., Multiparticle Production in Liquid Hydrogen by Charged Cosmic Hadrons of Energy Greater than 70 GeV (to be published).

7. Until now the only source of angular distributions from ultrahigh-energy collisions has been from the interactions of cosmic-ray hadrons with complex nuclei. However, this type of experiment has produced only a small number of events suitable for analysis, and these were obtained without a direct measurement of the incident energy.
8. L. Caneschi, D. E. Lyon, Jr., and Clifford Risk, Angular Distribution of Multiparticle Events at High Energy, Lawrence Radiation Laboratory Report UCRL-19814, 1970, submitted to Phys. Rev. Letters.
9. These three models actually predict $d^3N = f(p_T^2)\frac{d^3p}{E}$. However, Tow, in Ref.2, has shown numerically for the ABFST multiperipheral model that $f(p_T^2)$ is of the form $\exp(-Ap_T^2)$ (here we have ignored the small second bump in the p_T distribution found in this paper.)
10. In the lab system almost all events lie within 90 deg of the beam direction.
11. This flat lab distribution has raised doubt as to whether the multiperipheral model can explain the two bump structure observed in some cosmic ray events. However, O. Czyzewski and A. Krzywicki, Nuovo Cimento 30, 603 (1963), using a flat distribution in η to generate events by a Monte Carlo method, found that the experimental two-bump structure can be explained as statistical fluctuations of the multiperipheral flat distribution. Recently, E. I. Daibog and I. L. Rozental, Soviet J. Nucl. Phys. 10, 473 (1970), claimed that, using the momentum distribution $e^{-Bp_T}\frac{d^3p}{p_L}$, they get a two-bump distribution in the lab. However, they incorrectly evaluated the Jacobian by replacing dp_L with dp. If they had not made this replacement, they would get essentially the same distribution as ours for the case $m = 0$. They also claimed that Czyzewski and

Krzywicki made a mistake in changing from p_L to p by neglecting the two valued property of p_L. However, Czyzewski and Krzywicki made this approximation in the lab system, where p_L, except for a very small fraction of particles, is always of the same sign.

12. P. Ciok et al., Nuovo Cimento 8, 166 (1958); 10, 741 (1958); G. Cocconi, Phys. Rev. 111, 1699 (1958); K. Niu, Nuovo Cimento 10, 944 (1958).

13. J. Benecke, T. T. Chou, C. N. Yang, and E. Yen, Phys. Rev. 188, 2159 (1969).

FIGURE CAPTIONS

Fig. 1. Longitudinal momentum and angular distributions. Solid lines are predictions of Eq. (1) without phase-space corrections; dashed lines include phase-space corrections.

(a) $\frac{dN}{dp_L} = \frac{1}{E}$ in c.m.,

(b) $\frac{dN}{dp_L} = \frac{1}{E}$ in lab.,

(c) $\frac{dN}{d\eta_{cm}}$,

(d) $\frac{dN}{d\eta_\ell}$.

Fig. 2. $\frac{dN}{d\eta_{cm}}$ plot. The distribution is symmetric about $\eta_{cm} = 0$.

(a) p_{max}^{cm} varies, A and m are fixed;

(b) A varies, p_{max}^{cm} and m are fixed;

(c) m varies, p_{max}^{cm} and A are fixed.

Fig. 3. $\frac{dN}{d\eta}$ plot.

Fig. 4. Peyrou plot in c.m. Lines are level curves of constant density; numbers denote densities of particles per unit area along each curve.

Fig. 5. $\frac{dN}{dw}$ in lab system for two incident energies, with phase-space effects included by the method of Ref. 8. $\frac{dN}{dw}$ in c.m. is related to the lab distribution through Eq. (12) by a translation.

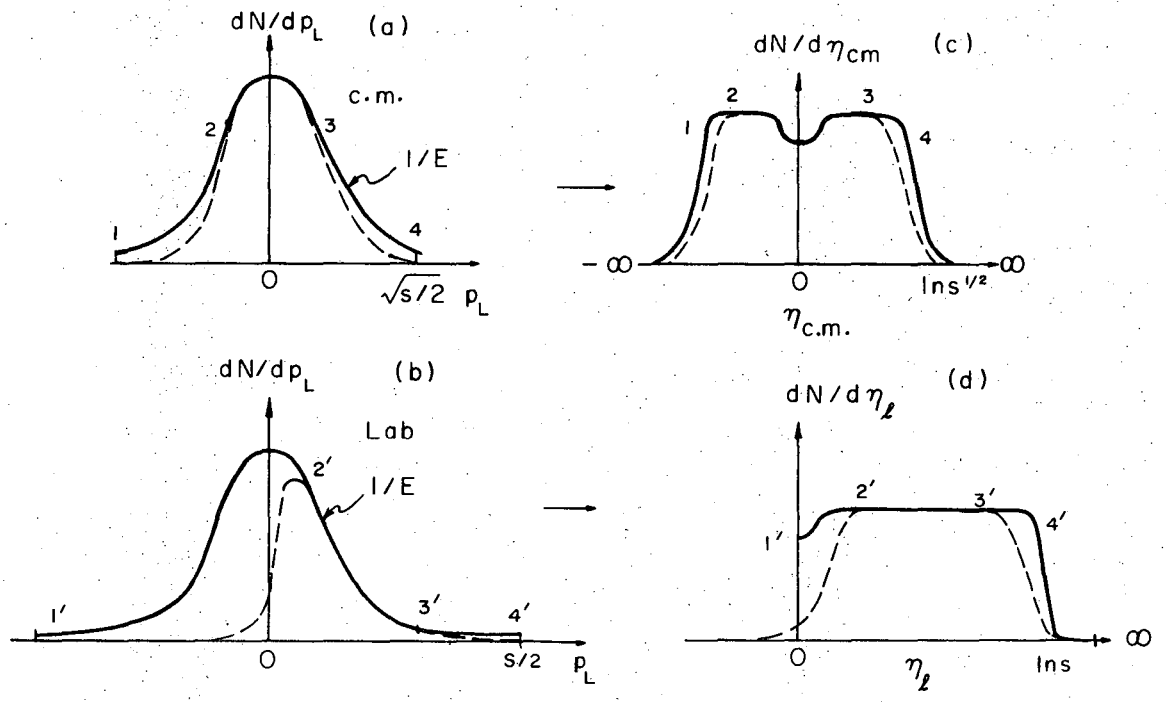
dN/dp_L
(a)
c.m.
1/E
1
2
3
4
0
√s/2 p_L
dN/dη_cm
(c)
−∞
0
ln s^1/2
∞
η_c.m.
dN/dp_L
(b)
Lab
1/E
1′
2′
3′
4′
0
s/2
p_L
dN/dη_ℓ
(d)
1′
2′
3′
4′
0
η_ℓ
ln s
∞
XBL707-3355

Fig. 1

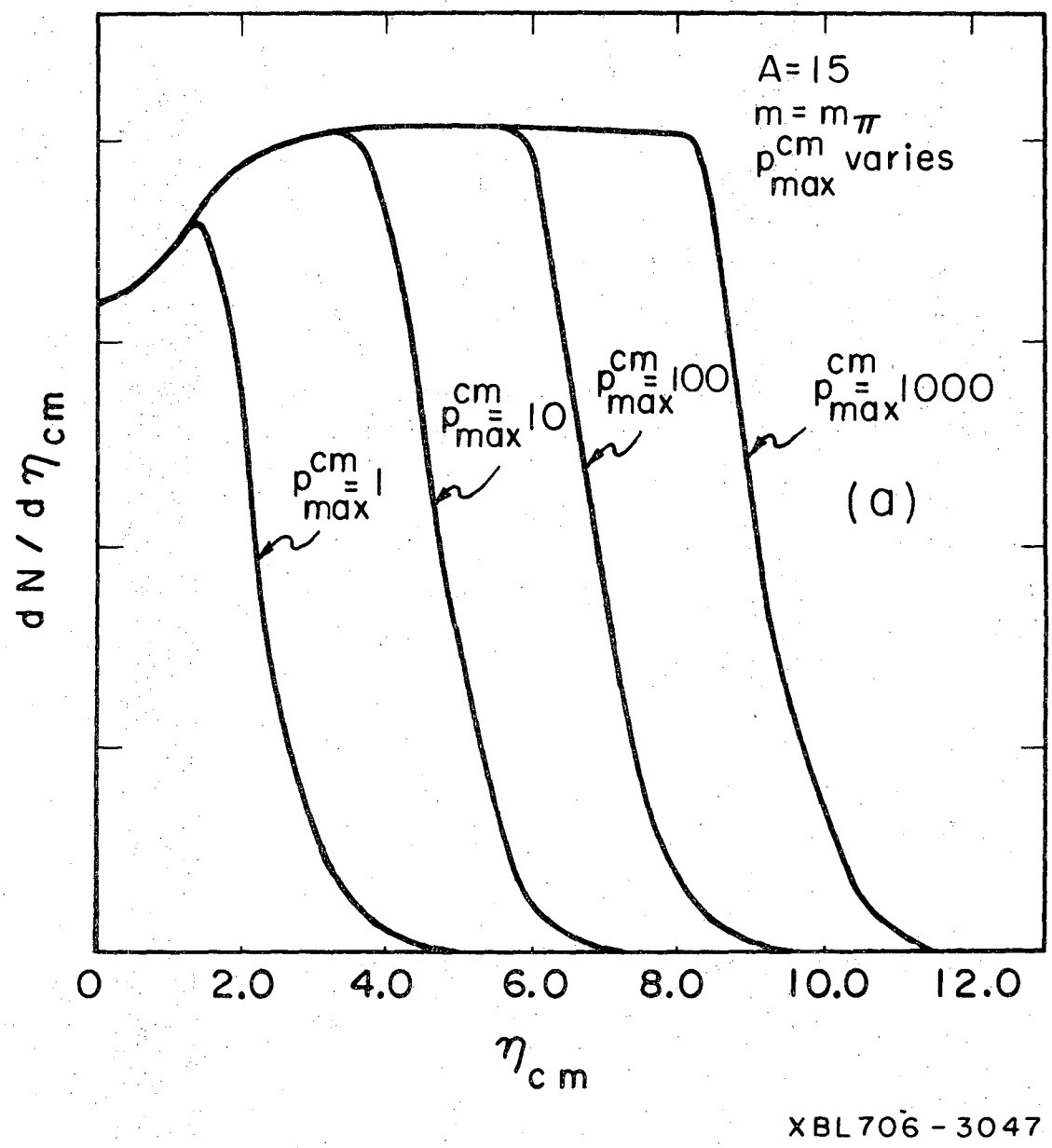
A=15
m = m_π
p^cm_max varies
p^cm_max 1
p^cm_max 10
p^cm_max 100
p^cm_max 1000
(a)
dN / dη_cm
η_cm
0
2.0
4.0
6.0
8.0
10.0
12.0
XBL706-3047

Fig. 2a

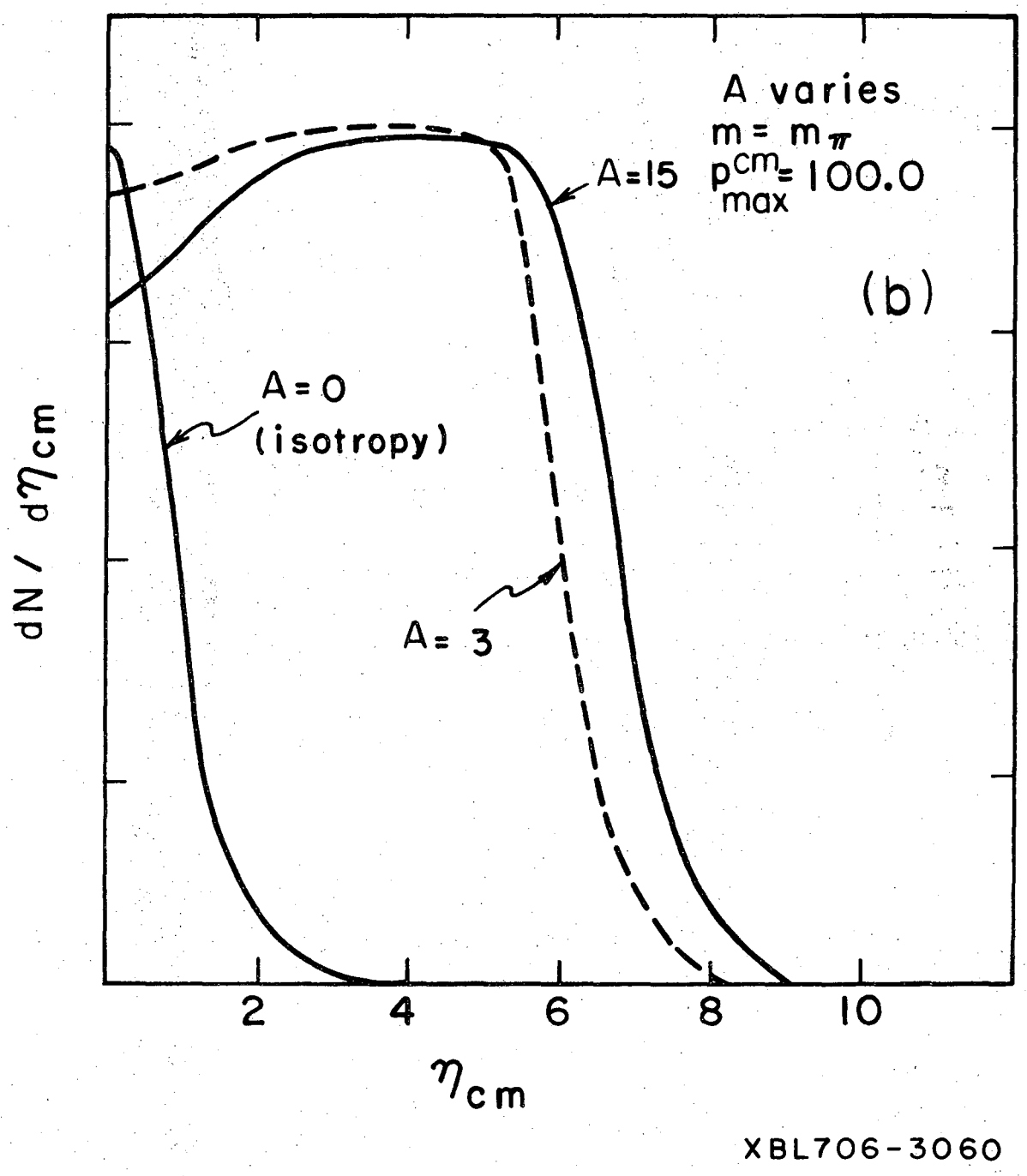
A varies
m = m_π
A=15 p^cm_max = 100.0
(b)
A=0
(isotropy)
A= 3
dN / dη_cm
2
4
6
8
10
η_cm
XBL706-3060

Fig. 2b

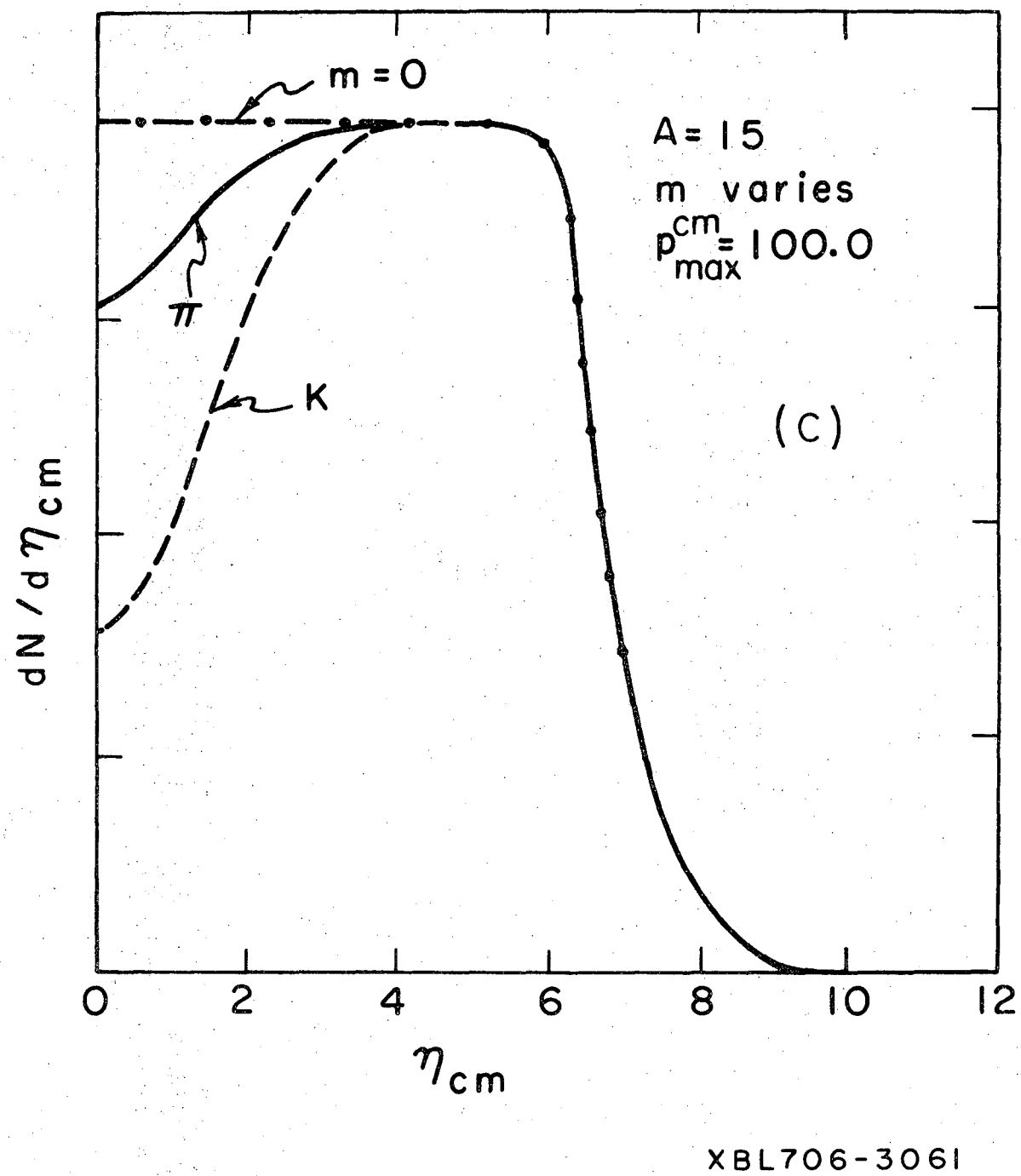
m = 0
A = 15
m varies
p^{cm}_{max} = 100.0
π
K
(C)
dN / dη cm
0
2
4
6
8
10
12
η cm
XBL706-3061

Fig. 2c

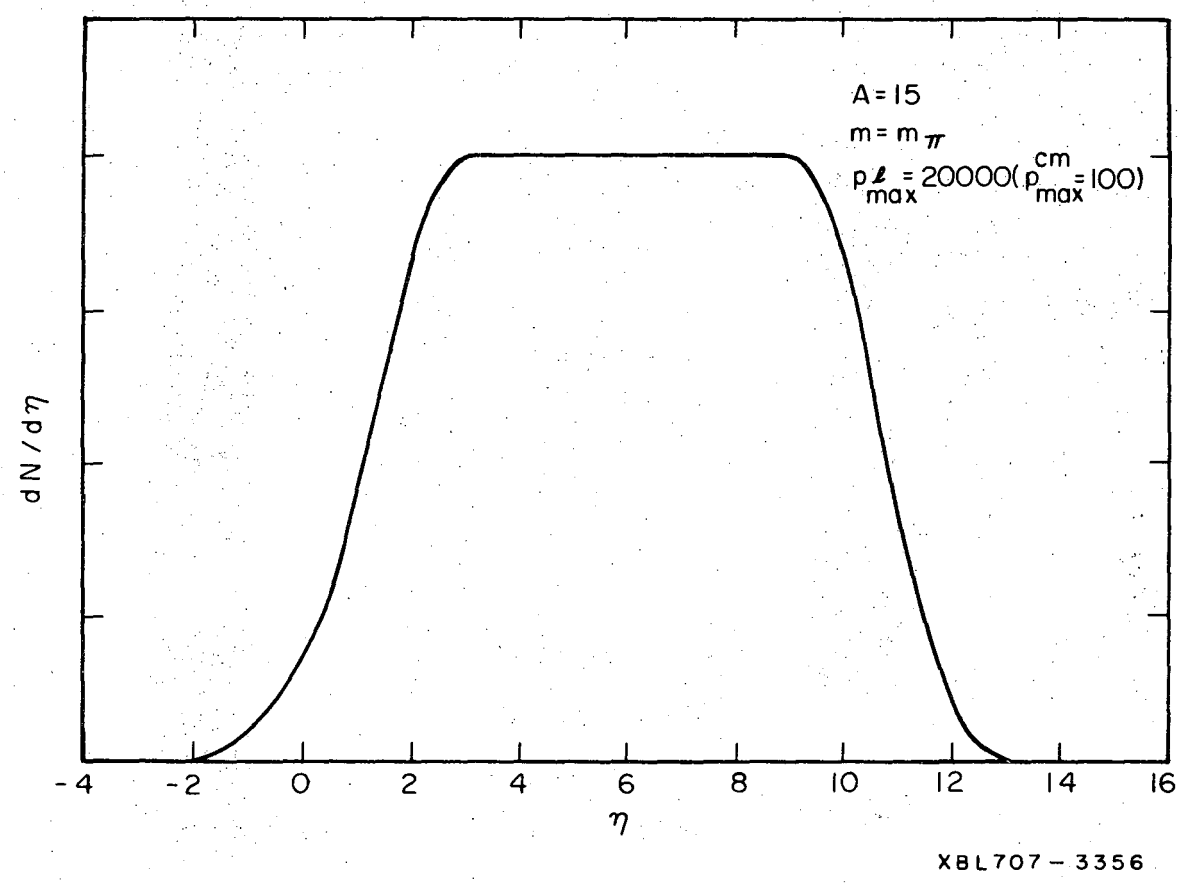
A = 15
m = m π
p ℓ max = 20000 (p cm max = 100)
dN / dη
-4
-2
0
2
4
6
8
10
12
14
16
η
XBL707-3356

Fig. 3

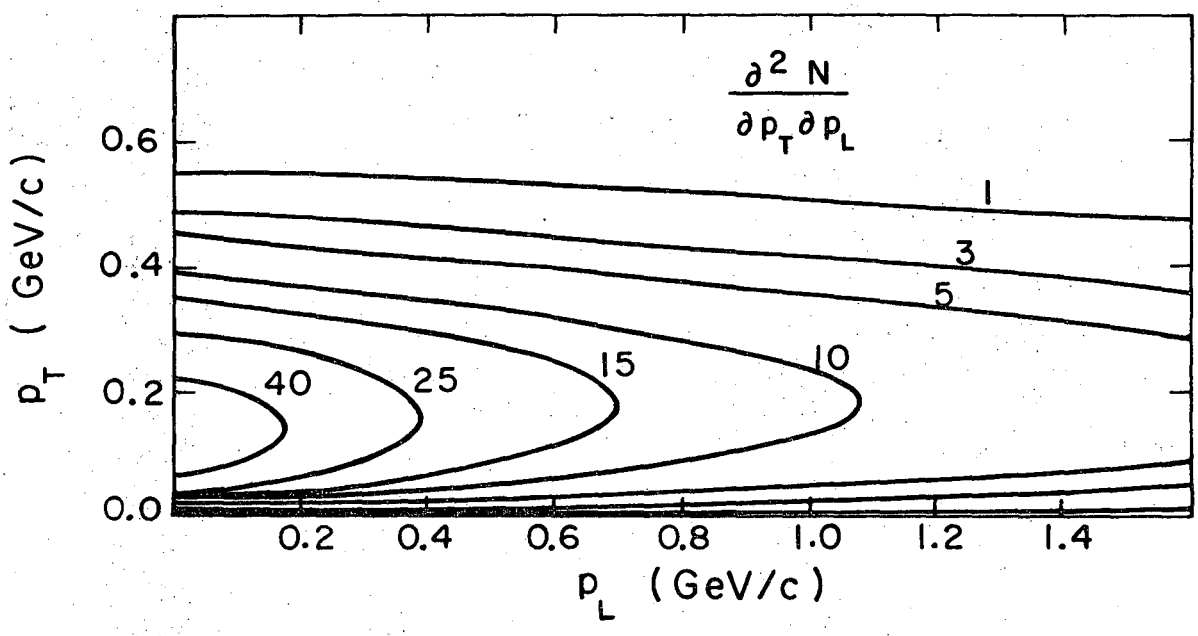

XBL706-3062

Fig. 4

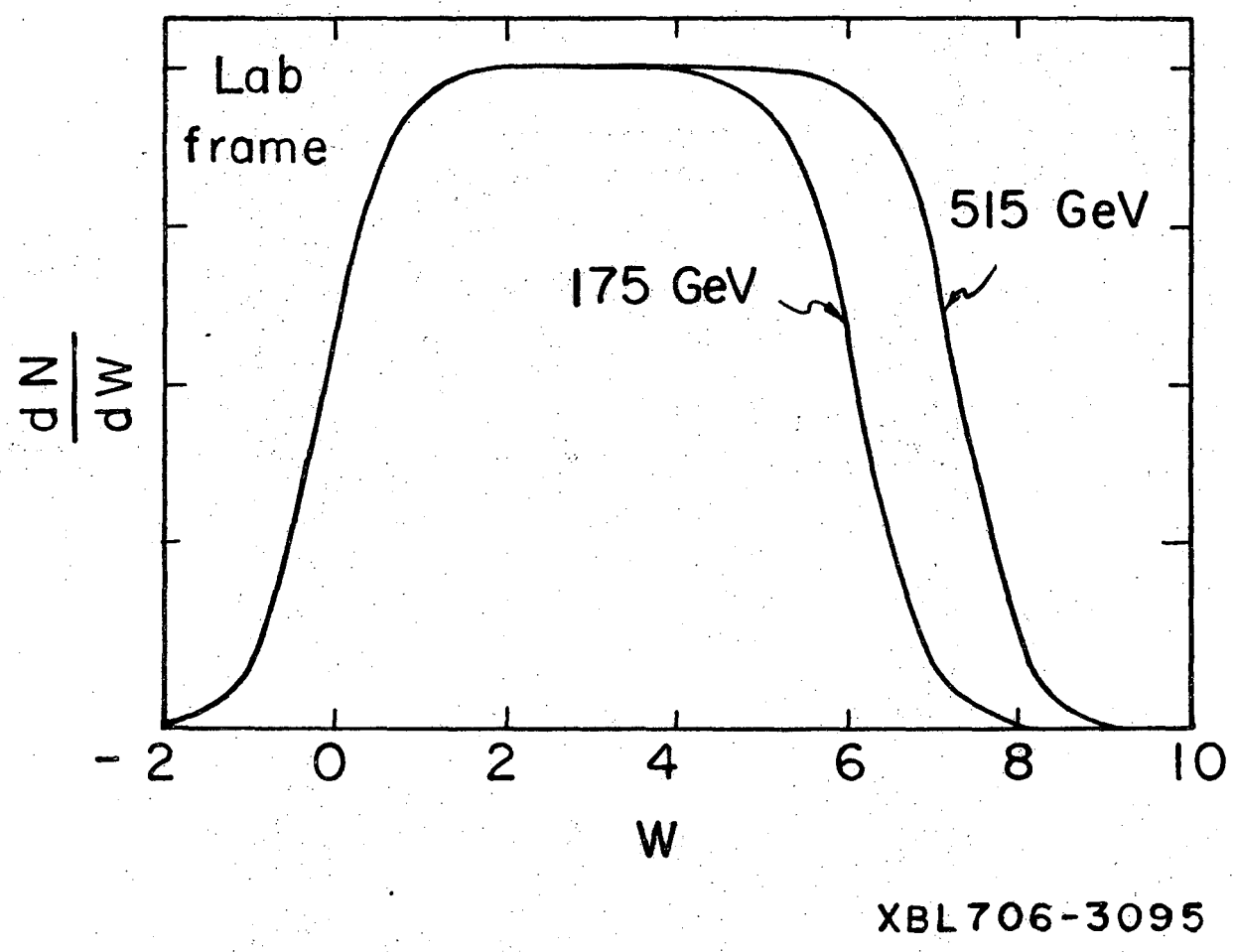

Fig. 5

TECHNICAL INFORMATION DIVISION
LAWRENCE RADIATION LABORATORY
UNIVERSITY OF CALIFORNIA
BERKELEY, CALIFORNIA 94720